

NeuralAnnot: Neural Annotator for in-the-wild Expressive 3D Human Pose and Mesh Training Sets

Gyeongsik Moon Kyoung Mu Lee

ASRI, Seoul National University, Korea

{mks0601, kyoungmu}@snu.ac.kr

Abstract

Recovering expressive 3D human pose and mesh from in-the-wild images is greatly challenging due to the absence of the training data. Several optimization-based methods have been used to obtain 3D human model fits from GT 2D poses, which serve as pseudo-groundtruth (GT) 3D poses and meshes. However, they often suffer from severe depth ambiguity while requiring long running time because of their per-sample optimization that only uses 2D supervisions and priors. The per-sample optimization optimizes a 3D human model on each sample independently; therefore, running it on a large number of samples consumes long running time. In addition, the absence of the 3D supervisions makes their framework suffer from depth ambiguity. To overcome the limitations, we present NeuralAnnot, a neural annotator that learns to construct in-the-wild expressive 3D human pose and mesh training sets. Our NeuralAnnot is trained on entire datasets by considering multiple samples together with additional 3D supervisions from auxiliary datasets; therefore, it produces far better 3D pseudo-GT fits much faster. We show that the newly obtained training set brings great performance gain, which will be publicly released with codes.

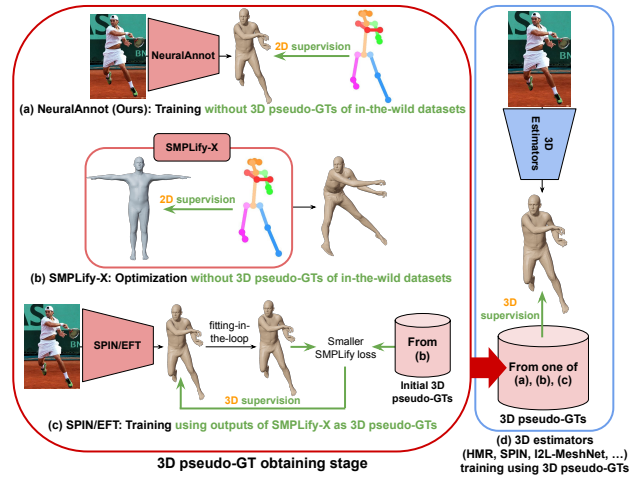


Figure 1: 3D human body pseudo-GT fit obtaining methods comparison. (a) and (b): NeuralAnnot and SMPLify-X can obtain 3D pseudo-GT fits from GT 2D pose without 3D pseudo-GT fits of in-the-wild datasets. (c): SPIN and EFT require initial 3D pseudo-GT fits of many datasets [2, 9, 11, 12, 23, 26], including in-the-wild datasets, for the training. It used the outputs of SMPLify-X as the initial 3D pseudo-GT fits; however, our NeuralAnnot can provide better ones. **Therefore, our direct comparison target is SMPLify-X.** (d): The obtained 3D pseudo-GT fits are used to train 3D estimators [15, 19, 28].

1. Introduction

Expressive 3D human pose and mesh estimation aims to localize joints and mesh vertices of all human parts, including body, hands, and face, simultaneously in the 3D space. By combining 3D pose and mesh of all human parts, we can understand not only human articulation and shape but also human intention and feeling, which can be useful in motion capture, virtual/augmented reality, and human action recognition. However, this is a very challenging task because of the complicated human body and hand articulations and the absence of an in-the-wild training set.

The 3D human pose and mesh data are usually obtained

by fitting a 3D human model (e.g., SMPL [25] for body, MANO [33] for hands, FLAME [22] for face, or SMPL-X [32] for all parts) to target data, such as 2D/3D pose or 3D point cloud. The 3D fits additionally contain 3D rotations of human joints and 3D human model parameters (e.g., latent codes of body shape and facial expression) compared with the above target data. Well-calibrated cameras or markers can provide 3D target data; however, setting those equipment takes high costs and efforts, which makes capturing the 3D target data from daily life at any time and any place very hard. Thus, most of the datasets that provide the 3D target data [9, 13, 26, 30, 38] are captured in special environ-

ments, such as multi-view studio, which have limited image appearance. Recent 3DPW dataset [36] obtained 3D human model fits from outdoor using 2D pose detections and IMU sensors; however, the appearance and pose diversity and the data scale are limited due to the difficulty of the capture.

Alternatively, optimization-based methods [4, 32] have been widely used to obtain 3D fits from in-the-wild images, which serve as pseudo-GT 3D poses and meshes. They perform a per-sample optimization, which fits a 3D human model to the GT 2D pose of each sample independently, only using 2D supervisions. Although they work well when the target pose is similar to the initial one and has a small depth ambiguity, such as 3D face fitting, they often produce inaccurate and implausible 3D body/hand fits. Also, they suffer from a long running time. The first reason for the limitations is that their per-sample optimization considers each sample independently; therefore, it takes a large amount of time when there are many samples and can be easily stuck in local minima. Second, their frameworks are optimized using only 2D supervisions and heavily rely on prior terms to prevent implausible poses. Complicated articulations of the human body and hand make the optimization hard without using 3D supervisions.

To overcome the limitations of the optimization-based methods, we present *NeuralAnnot*, a neural annotator that learns to construct in-the-wild expressive 3D human pose and mesh training sets. Our *NeuralAnnot* takes a single RGB image and outputs 3D human model parameters [25, 32, 33], which becomes a 3D pseudo-GT fit of the input image. It is trained on entire datasets, not on each sample independently, by updating its learnable weights from multiple samples. Therefore, *NeuralAnnot* takes a much shorter running time while it is much more robust to the local minima. In addition, our *NeuralAnnot* is jointly trained using 2D supervisions from a target in-the-wild dataset and 3D supervisions from auxiliary datasets. We use datasets that provide GT 3D pose but captured from restricted lab environments as the auxiliary datasets. Under the joint training, 2D supervisions from the in-the-wild dataset make *NeuralAnnot* generalize well to diverse image appearance, and 3D supervisions from the auxiliary dataset make *NeuralAnnot* learn how to recover depth information from the 2D input.

Figure 1 shows 3D human body pseudo-GT fit obtaining methods comparison. As *NeuralAnnot* and SMPLify-X [32] produce 3D pseudo-GT fits without 3D fits of in-the-wild datasets, our direct comparison target is SMPLify-X. We will release the newly obtained pseudo-GTs of in-the-wild dataset [10, 23] and codes for the continual study of expressive 3D human pose and mesh estimation in the wild. In addition, we will apply *NeuralAnnot* to most of the existing human body/hand/face datasets [1, 3, 9, 11, 16, 23, 26, 27, 30, 36, 39] and release all 3D pseudo-GT fits.

Our contributions can be summarized as follows.

- We present *NeuralAnnot*, a neural annotator that learns to construct in-the-wild expressive 3D human pose and mesh training sets. Our *NeuralAnnot* is trained on entire datasets by considering multiple samples together with additional 3D supervisions from the auxiliary datasets.
- Our *NeuralAnnot* produces far better 3D pseudo-GT fits with a much shorter running time than previous optimization-based methods, and the newly obtained training set brings great performance gain.
- The newly obtained pseudo-GT expressive and part-specific 3D human poses and meshes will be publicly released. We believe the new pseudo-GTs will be highly beneficial to the community.

2. Related works

Training sets for 3D human pose and mesh estimation.

There are two types of training sets for 3D human pose and mesh estimation. Datasets of the first type [2, 11, 12, 23] are captured in the wild without special devices, such as calibrated cameras and markers. As no special devices are required, those datasets contain images with diverse appearance with GT 2D pose, usually obtained by manual human annotations. However, due to the depth and scale ambiguity, a single view image in those datasets cannot provide GT 3D pose. Datasets of the second type [9, 13, 26, 30, 41] are captured from restricted lab environments with well-calibrated cameras or markers. The restricted environment makes the datasets contain images with monotonous appearance; however, multi-view images or marker data provide GT 3D pose. From the GT 2D/3D poses, optimization-based annotators have been widely used to obtain 3D pseudo-GT human model fits. Our *NeuralAnnot* is proposed to obtain 3D pseudo-GT fits more effectively and efficiently than previous annotators.

Optimization-based 3D pseudo-GT annotators. The optimization-based methods have been widely used to obtain 3D pseudo-GT fits. SMPLify [4] fits a 3D human body model (*i.e.*, SMPL [25]) to a given 2D pose by minimizing 2D pose loss and several prior terms. SMPLify-X [32] is in a similar spirit to SMPLify, and they extended SMPLify for the expressive 3D human model fitting by proposing a new expressive 3D human model, SMPL-X. Kulon *et al.* [20] collected pseudo-GT 3D hands from in-the-wild videos by fitting the MANO to 2D hand joint detections.

Compared with the above optimization-based methods [4, 32], our *NeuralAnnot* has clear novel and strong points. First, ours is much more robust to the local minima and much faster than the above methods because ours

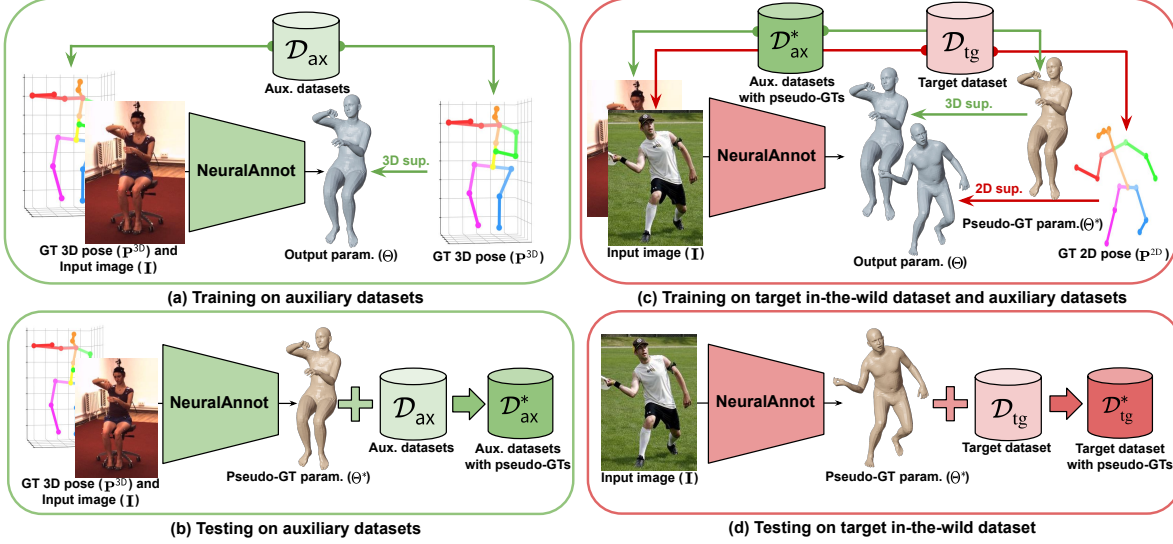


Figure 2: Overall pipeline of NeuralAnnot. (a) We first train NeuralAnnot on the auxiliary datasets that provide GT 3D pose. (b) After the training, testing results on the auxiliary datasets become 3D pseudo-GT fits of the datasets. (c) Another NeuralAnnot is jointly trained on the auxiliary datasets with the 3D pseudo-GT fits and the target in-the-wild dataset. (d) After the training, testing results on the target in-the-wild dataset become 3D pseudo-GT fits of the dataset.

is trained on entire datasets by considering multiple samples together while they perform the per-sample optimization. In particular, the above methods are prone to noisy target 2D/3D pose, truncation, and poses that are far from the initial zero poses of 3D human models. Second, ours gets benefits from 3D supervisions using auxiliary datasets that provide GT 3D pose, while they only rely on 2D supervisions and priors when obtaining 3D pseudo-GT fits.

Neural network-based 3D pseudo-GT annotators. Recently, EFT [14] has been introduced to obtain 3D pseudo-GT fits. EFT [14] fine-tunes a pre-trained 3D human pose and mesh estimation network, SPIN [18], to the GT 2D pose of each training image. There are two critical differences between the NeuralAnnot and EFT [14]. First, NeuralAnnot does not require prepared 3D pseudo-GT fits of in-the-wild datasets. On the other hand, EFT [14] requires initial 3D pseudo-GT fits of many datasets [2, 9, 11, 12, 23, 26], including in-the-wild datasets, to train their base network [18]. EFT [14] obtained the initial 3D pseudo-GT fits using optimization-based methods [4, 32], which takes a large amount of time. Here, our NeuralAnnot can be used to obtain the initial 3D pseudo-GT fits more effectively and efficiently than the widely used optimization-based annotators. Second, EFT assumes a well-performing pre-trained network is available, which is not applicable to expressive 3D human pose and mesh estimation as only several recent methods [6, 29] have been proposed to address this problem. In contrast, ours do not require any well-performing pre-trained networks.

Several 3D human pose and mesh estimation methods can be used to obtain 3D pseudo-GT fit as they do not

require 3D pseudo-GT fits of in-the-wild datasets for the training. SPIN [18] reported their networks can be trained in an unpaired setting, which does not require pairs of images and 3D pseudo-GT fits, by utilizing a large pool of 3D fits without images. Although the unpaired training is possible, we show that paired 3D pseudo-GT fits are necessary for them to achieve the best annotation performance in the experimental section, where the paired 3D pseudo-GT fits can be obtained by our NeuralAnnot. Song *et al.* [35] presented a network that learns to fit the output 3D pose and mesh to the target 2D pose. As their network takes a 2D pose as an input, they used motion capture datasets for the training, which contains a number of 3D fits without images. However, their 2D pose input makes their network suffer from depth ambiguity and output wrong 3D pseudo-GT fits from a truncated input, which will be shown in the experiment section. On the other hand, our image input makes NeuralAnnot relatively more robust to the depth ambiguity and truncation.

3. NeuralAnnot

NeuralAnnot predicts 3D human model parameters Θ from a single image I . We design NeuralAnnot as a simple combination of ResNet [8] and a regressor, which extracts image feature vector F and regresses a set of 3D human model parameters Θ , respectively. F is obtained by performing global average pooling on the ResNet output feature. The regressor consists of several fully connected layers, and the 3D human model parameter set is different for each human model, which will be described in Section 4. The 3D human pose and mesh can be obtained from Θ us-

Algorithm 1 Neural annotation

Input: \mathcal{D}_{ax} : Auxiliary datasets with GT 3D pose

Input: \mathcal{D}_{tg} : Target in-the-wild dataset with GT 2D pose

Output: $\mathcal{D}_{\text{ax}}^*$: \mathcal{D}_{ax} and predicted pseudo-GTs

Output: $\mathcal{D}_{\text{tg}}^*$: \mathcal{D}_{tg} and predicted pseudo-GTs

```
1: for  $n \leftarrow 1$  to  $N_{\text{ax}}$  do
2:   Randomly initialize NeuralAnnot
3:   Train NeuralAnnot on  $\mathcal{D}_{\text{ax},n}$  by minimizing  $L_{\text{ax}}$ 
4:   Test NeuralAnnot on all images of  $\mathcal{D}_{\text{ax},n}$ 
5:    $\mathcal{D}_{\text{ax},n}^* = \{\mathcal{S} \hat{\cap} \Theta^* | \mathcal{S} \in \mathcal{D}_{\text{ax},n}\}$ 
6: end for
7: Randomly initialize NeuralAnnot
8: Train NeuralAnnot on  $\mathcal{D}_{\text{tg}}$  and  $\mathcal{D}_{\text{ax}}^*$  by minimizing  $L_{\text{tg}}$ 
9: Test NeuralAnnot on all images of  $\mathcal{D}_{\text{tg}}$ 
10:  $\mathcal{D}_{\text{tg}}^* = \{\mathcal{S} \hat{\cap} \Theta^* | \mathcal{S} \in \mathcal{D}_{\text{tg}}\}$ 
```

ing 3D human models [22, 25, 32, 33].

The procedure of the neural annotation is described in Algorithm 1. NeuralAnnot is jointly trained on a target in-the-wild dataset with GT 2D pose $\mathcal{D}_{\text{tg}} = \{(\mathbf{I}_s, \mathbf{P}_s^{2D})\}_{s=1}^{S_{\text{tg}}}$ and auxiliary datasets with GT 3D pose $\mathcal{D}_{\text{ax}} = \{\mathcal{D}_{\text{ax},n}\}_{n=1}^{N_{\text{ax}}}$. S_{tg} and N_{ax} denote the number of data samples in \mathcal{D}_{tg} and the number of auxiliary datasets, respectively, and $\mathcal{D}_{\text{ax},n} = \{(\mathbf{I}_s, \mathbf{P}_s^{2D}, \mathbf{P}_s^{3D})\}_{s=1}^{S_{\text{ax},n}}$. \mathbf{I} , \mathbf{P}^{2D} , \mathbf{P}^{3D} , and $S_{\text{ax},n}$ denote image, GT 2D pose, GT 3D pose, and the number of data samples in $\mathcal{D}_{\text{ax},n}$, respectively. To this end, we first obtain pseudo-GT 3D human model parameters of the auxiliary datasets, thus \mathcal{D}_{ax} becomes $\mathcal{D}_{\text{ax}}^* = \{\mathcal{D}_{\text{ax},n}^*\}_{n=1}^{N_{\text{ax}}}$, where $\mathcal{D}_{\text{ax},n}^* = \{\mathcal{S} \hat{\cap} \Theta^* | \mathcal{S} \in \mathcal{D}_{\text{ax},n}\}$. Then, the auxiliary datasets with the obtained pseudo-GTs $\mathcal{D}_{\text{ax}}^*$ are used to obtain pseudo-GT 3D human model parameters of the target in-the-wild dataset, thus \mathcal{D}_{tg} becomes $\mathcal{D}_{\text{tg}}^* = \{\mathcal{S} \hat{\cap} \Theta^* | \mathcal{S} \in \mathcal{D}_{\text{tg}}\}$, as shown in Figure 2. $\hat{\cap}$ and Θ^* denote tuple extension¹ and predicted 3D human model parameters from \mathbf{I} in \mathcal{S} after the training, which is a 3D pseudo-GT fit, respectively. We provide detailed descriptions of how to obtain pseudo-GT 3D human pose and mesh from the auxiliary and target datasets below.

3.1. 3D pseudo-GT fits of datasets with GT 3D pose

The regressor takes a pair of image feature \mathbf{F} and GT 3D pose \mathbf{P}^{3D} when NeuralAnnot is trained to predict pseudo-GTs of the auxiliary datasets that provide GT 3D pose \mathcal{D}_{ax} [9, 26, 30]. The image feature provides human articulation and shape information, while GT 3D pose additionally provides depth and real scale information, which lacks in the 2D image feature. To this end, the GT 3D pose \mathbf{P}^{3D} is converted to a 512-dimensional feature by two fully connected layers and concatenated with global average pooled ResNet output feature \mathbf{F} . The concatenated feature is fed

to a fully connected layer for the 3D human model parameter regression. The 3D rotations of joints in the predicted 3D human model parameters are initially predicted in a 6D rotational representation of Zhou *et al.* [40] and converted to a 3D axis-angle rotation. The loss function is defined as follows:

$$L_{\text{ax}} = \|\hat{\mathbf{P}}^{3D} - \mathbf{P}^{3D}\|_1 + \sum_{\theta \in \Theta} \lambda_{\text{ax},\theta} \hat{\theta}^2,$$

where the hat mark indicates a predicted output. $\hat{\mathbf{P}}^{3D}$ is obtained from 3D human model layer. $\lambda_{\text{ax},\theta}$ denotes $L2$ norm regularizer weight of each 3D human parameter θ . The $L2$ norm regularizer prevents implausible 3D human pose and mesh. After the training, the testing results on all images of the dataset become new pseudo-GTs of the dataset, which form $\mathcal{D}_{\text{ax},\bullet}^*$.

3.2. 3D pseudo-GT fits of in-the-wild datasets

The regressor outputs 3D human model parameters from the image feature \mathbf{F} when NeuralAnnot is trained to predict pseudo-GTs of in-the-wild datasets that do not provide GT 3D pose \mathcal{D}_{tg} [23]. The most important contribution of our NeuralAnnot is that we use the auxiliary datasets with the obtained pseudo-GTs $\mathcal{D}_{\text{ax}}^*$ for the pseudo-GTs of a target in-the-wild dataset \mathcal{D}_{tg} . To this end, we make a mini-batch of each iteration from multiple datasets, including the auxiliary datasets $\mathcal{D}_{\text{ax}}^*$ and the target in-the-wild dataset \mathcal{D}_{tg} . Thus, our NeuralAnnot is jointly trained on the auxiliary datasets and target in-the-wild dataset and can benefit from the 3D supervisions from the auxiliary datasets.

Although samples from the auxiliary datasets can benefit NeuralAnnot by the 3D supervisions, samples from the target in-the-wild datasets are supervised only using GT 2D pose. To prevent implausible 3D human pose and mesh induced by the 2D supervisions, NeuralAnnot predicts a low-dimensional embedding of the 3D rotations (*i.e.*, a latent code of VPoser [32] for the body part and PCA coefficients for the hand part [33]), following SMPLify-X [32], unlike directly predicting 3D rotations when trained to output pseudo-GTs of the auxiliary datasets \mathcal{D}_{ax} . The low-dimensional embedding can effectively limit the 3D human pose and mesh to plausible articulation space, thus can prevent implausible 3D human pose and mesh. Note that the low-dimensional embeddings can be learned from $\mathcal{D}_{\text{ax}}^*$, if not available. The loss function is defined as follows:

$$L_{\text{tg}} = \|\hat{\mathbf{P}}^{2D} - \mathbf{P}^{2D}\|_1 + \mathbb{1}_{\text{tg}} \sum_{\theta \in \Theta} \lambda_{\text{tg},\theta} \hat{\theta}^2 + (1 - \mathbb{1}_{\text{tg}}) (\|\hat{\mathbf{P}}^{3D} - \mathbf{P}^{3D}\|_1 + \sum_{\theta \in \Theta} \|\hat{\theta} - \theta^*\|_1),$$

where the hat mark indicates a predicted output. θ^* is from Θ^* . $\lambda_{\text{tg},\theta}$ denotes $L2$ norm regularizer weight of each 3D

¹ $(a, b) \hat{\cap} c = (a, b, c)$

human model parameter θ for samples from the target in-the-wild dataset. The $L2$ norm regularizer prevents implausible 3D human pose and mesh. $\mathbb{1}_{\text{tg}}$ is 1 when a sample is from target in-the-wild dataset \mathcal{D}_{tg} and zero otherwise. After the training, the testing results on all images of the target in-the-wild dataset become new pseudo-GTs of the dataset, which form $\mathcal{D}_{\text{tg}}^*$.

4. Expressive 3D pseudo-GT fits

For the expressive 3D pseudo-GTs, we design separated networks for the body and hand parts, as shown in Figure 3, where the networks are trained independently. This separation enables us to obtain part-specific pseudo-GTs as well as expressive ones.

Body part. The body part predicts SMPL/SMPL-X parameters, including 3D body global rotation $\theta_b^g \in \mathbb{R}^3$, 3D body rotations $\theta_b \in \mathbb{R}^{21 \times 3}$, shape parameter $\beta_b \in \mathbb{R}^{10}$, and camera parameter $k_b \in \mathbb{R}^3$. It predicts SMPL parameters when we want only body part pseudo-GTs. We set Θ to $\{\theta_b, \beta_b\}$ and $\{z_b, \beta_b\}$ when training NeuralAnnot to minimize L_{ax} and L_{tg} , respectively. z_b denotes the latent code of the VPoser [32].

Hand part. The hand part outputs MANO parameters, including 3D hand global rotation $\theta_h^g \in \mathbb{R}^3$, 3D hand rotations $\theta_h \in \mathbb{R}^{15 \times 3}$, shape parameter $\beta_h \in \mathbb{R}^{10}$, and camera parameter $k_h \in \mathbb{R}^3$. All hand images are flipped to the right hands, and we flip back the estimated pseudo-GTs of the left hands. We set Θ to $\{\theta_h, \beta_h\}$ and $\{z_h, \beta_h\}$ when training NeuralAnnot to minimize L_{ax} and L_{tg} , respectively. z_h denotes the 3D hand pose PCA coefficients, defined in MANO.

Face part. For the face, we use SMPLify-X [32] to obtain pseudo-GT 3D face model parameter instead of using NeuralAnnot because not complicated articulations of the face make SMPLify-X work well. We modified SMPLify-X to fit FLAME on GT 2D face keypoints. The original loss functions, including keypoint loss and a set of priors, are used for the fitting. It optimizes 3D face global rotation $\theta_f^g \in \mathbb{R}^3$, 3D jaw rotation $\theta_f \in \mathbb{R}^3$, shape parameter $\beta_f \in \mathbb{R}^{10}$, and expression code $\psi \in \mathbb{R}^{10}$.

Integration to expressive 3D pseudo-GTs. After obtaining the part-specific pseudo-GTs, the final expressive 3D pseudo-GTs are obtained by forwarding $\{\theta_b^g, \theta_b, \beta_b, \theta_{rh}, \theta_{lh}, \theta_{lh}, \theta_{lh}, \theta_f, \psi\}$ to SMPL-X, where $*_{rh}$ and $*_{lh}$ denote $*$ is from right and left hand, respectively. The 3D hand pose parameter θ_h of MANO and 3D jaw rotation θ_f and face expression code ψ of FLAME are compatible with those of SMPL-X; thus, we use them for the final expressive 3D pseudo-GTs. As the body part often predicts wrong rotations of elbows and wrists in the roll axis, we selectively use the 3D hand global rotation θ_h^g to replace rotations of the elbows and wrists based on a simple heuristic described in the supplementary material.

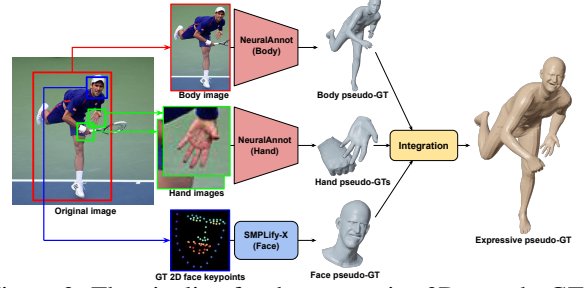


Figure 3: The pipeline for the expressive 3D pseudo-GTs.

5. Implementation details

PyTorch [31] is used for implementation. The backbone part is initialized with the publicly released ResNet50 [8], pre-trained on ImageNet [34]. The weights are updated by the Adam optimizer [17] with a mini-batch size of 192. Each mini-batch consists of half samples from the auxiliary datasets and half samples from the target in-the-wild dataset. All input images are cropped using groundtruth box and resized to 256×256 . No data augmentation is performed. The initial learning rate is set to 10^{-4} and reduced by a factor of 10 when it converges.

6. Experiment

6.1. Datasets

Datasets. For the body part, we use Human3.6M [9], MPI-INF-3DHP [26], and 3DPW [36] as the auxiliary datasets. For the hand part, FreiHAND [41] and InterHand2.6M [30] are used as the auxiliary dataset. For all parts, we use the whole-body version of MSCOCO [10, 23] as the target in-the-wild dataset. The expressive 3D pseudo-GTs are obtained by integrating part-specific ones of MSCOCO [10, 23].

6.2. Evaluation metrics

Annotation time. The annotation time represents how much time is required for the whole annotation procedure. For a fair comparison, the annotation time of the optimization-based annotators [4, 32] is measured from a quarter of all data samples as NeuralAnnot uses four GPUs for the training. The annotation time of NeuralAnnot is a summation of training and testing time, and we set the mini-batch size to 1 during the testing stage to simulate the per-sample optimization of the optimization-based annotators [4, 32].

Direct 3D annotation error. The direct 3D annotation error is defined as the average 3D joint distance (mm) between GT 3D poses and the pseudo-GTs. This metric is only applicable to datasets that provide GT 3D pose.

Indirect 3D annotation error. The indirect 3D annotation error represents how much the pseudo-GTs are beneficial

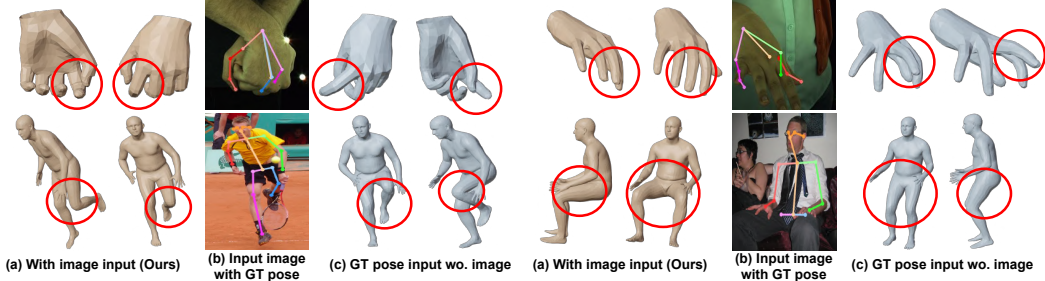


Figure 4: Qualitative comparison of 3D hand/body pseudo-GTs between models with and without an image input.

Auxiliary datasets	Indirect 3D err.
Human body part	PA MPJPE↓
None	69.6 (Unpaired setting of SPIN [18])
Human3.6M [9]	66.1
3DPW [36]	68.0
MPI-INF-3DHP [26]	65.9
All (Ours)	64.9
Human hand part	AUC↑
None	0.758 (Unpaired setting of SPIN [18])
FreiHAND [41]	0.779
InterHand2.6M [30]	0.772
All (Ours)	0.780

Table 1: Indirect 3D annotation errors comparison between various MSCOCO pseudo-GTs of body and hand parts.

for the training. The absence of the GT 3D pose of the in-the-wild datasets makes calculating the direct 3D annotation error impossible. Alternatively, we train a state-of-the-art 3D human pose and mesh estimator, I2L-MeshMet [28], on the obtained pseudo-GTs of the target in-the-wild dataset and use 3D testing errors on existing outdoor benchmarks as the indirect 3D annotation error. 3DPW [36] and FreiHAND [41] are used for the testing benchmarks for the body and hand parts, respectively. We split the FreiHAND training set into training and validation sets and report the results on the validation set. The error of the estimator is measured using the most widely used metrics, (PA) MPJPE (mm) and (PA) MPVPE (mm), and area under the curve (AUC). We provide more analysis using different estimators in the supplementary material.

6.3. Ablation study

Benefit of 3D supervisions from the auxiliary datasets.

Table 1 shows the 3D supervisions from the auxiliary datasets improve the indirect 3D annotation error. The settings without auxiliary datasets are similar to the unpaired setting of SPIN [18], which does not require paired images and 3D pseudo-GT fits. The large number of unpaired 3D pseudo-GT fits are used for the low-dimensional embedded pose (*i.e.*, VPoser [32] for the body and PCA coefficients for the hand). For each row of the table, NeuralAnnot uses the auxiliary datasets of the row and outputs pseudo-GTs of the target dataset following Algorithm 1. By using all aux-

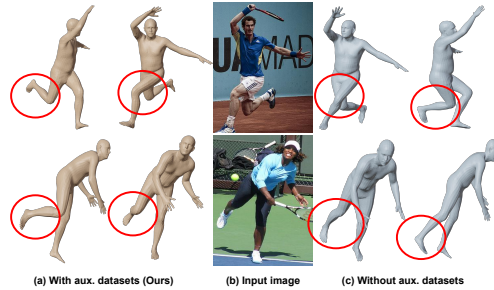


Figure 5: Qualitative comparison of 3D body pseudo-GTs between models with and without the auxiliary datasets.

Inputs	2D err.	Indirect 3D err.
GT 2D pose [5, 35]	7.2	69.4
Image (Ours)	8.1	65.9

Table 2: 2D annotation error (pixel) and indirect 3D annotation error (PA MPJPE) comparison between MSCOCO pseudo-GTs from NeuralAnnot that take different inputs.

iliary datasets, NeuralAnnot achieves the best indirect 3D annotation error. In particular, NeuralAnnot achieves much better indirect 3D annotation errors than the unpaired setting of SPIN [18], which shows the necessity of the 3D supervisions from the auxiliary datasets. Note that their paired setting requires initial 3D pseudo-GT fits of many datasets, which can be obtained by NeuralAnnot. Figure 5 shows the 3D supervisions are useful to alleviate the depth ambiguity.

Inputs of NeuralAnnot. Figure 4 shows that the image input plays a significant role for the high-quality pseudo-GTs. The top row shows the comparison between models that 1) take an image and GT 3D pose as input (ours) and 2) take only GT 3D pose on InterHand2.6M. The comparison shows that taking an image as input is greatly helpful to recover partially missing GT 3D pose, which arises from the failure of the marker-less data capture. The bottom row shows the comparison between models that 1) take an image as input (ours) and 2) take only GT 2D pose like Song *et al.* [35] on MSCOCO. The comparison shows that a model that takes only GT 2D pose suffers from more depth ambiguity, missing annotations, and truncation. On the other hand, the image input can provide depth order information by a body part occlusion, shadow, and perspective distortion (*e.g.*, in the first column, the shadow and small size

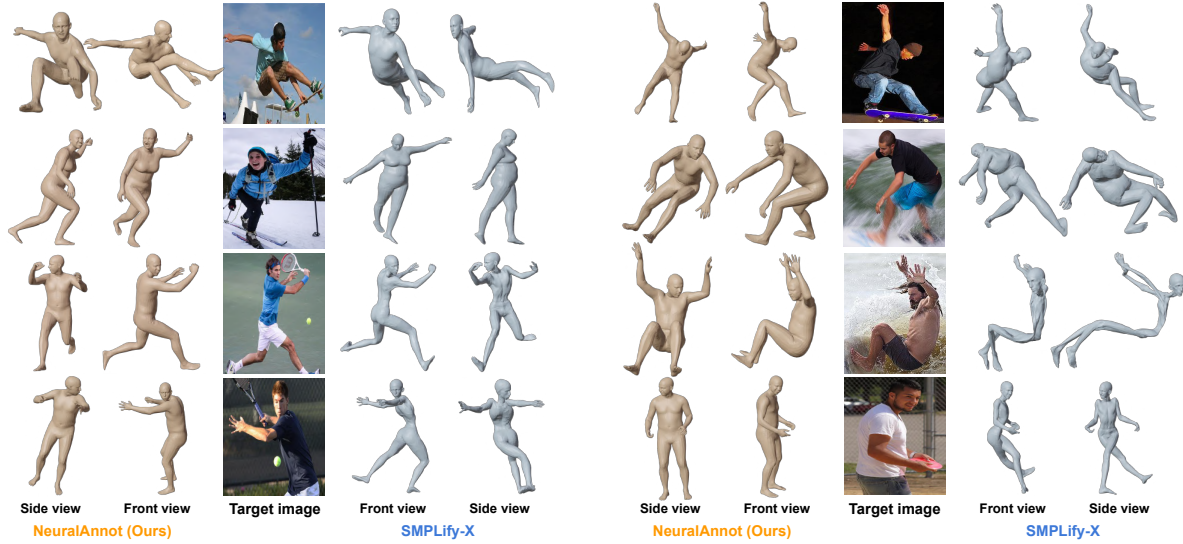


Figure 6: Qualitative comparison of expressive 3D pseudo-GT on challenging or truncated poses between NeuralAnnot and SMPLify-X.

Datasets	SMPLify-X [32]		NeuralAnnot (Ours)	
	Direct 3D err.	Time	Direct 3D err.	Time
Human body part				
Human3.6M [9]	13.1	12 days	9.8	7 hours
MPI-INF-3DHP [26]	17.9	5 days	16.4	3 hours
Human hand part				
InterHand2.6M [30]	10.0	3 days	5.8	2 hours

Table 3: The direct 3D annotation error and annotation time comparison between SMPLify-X and our NeuralAnnot on various datasets.

of the left knee tell us that the leg is behind the right leg). In addition, the image input can provide contextual information, helpful when annotations are missing or truncated. Table 2 further shows that pseudo-GTs from the image input achieves the lowest indirect 3D annotation error. We observed that using both an image and GT 2D pose as inputs marginally affects the indirect 3D error of a model that takes an image as an input. We think this is because the GT 2D pose does not carry depth information. The 2D annotation error is a pixel distance between GT 2D pose and the projected 2D pose from the pseudo-GTs.

6.4. Comparison with previous annotators

3D pseudo-GT fits of datasets with GT 3D pose. Table 3 and Figure 7 show that NeuralAnnot requires much less annotation time, while achieving lower direct 3D annotation error than SMPLify-X [32] on various datasets that provide GT 3D pose. The better performance is from the training on entire datasets by considering multiple samples together, while SMPLify-X optimizes their framework on each sample independently. Moreover, NeuralAnnot can recover pseudo-GTs from partially missing and noisy GT 3D pose by utilizing image features, as shown in the first row

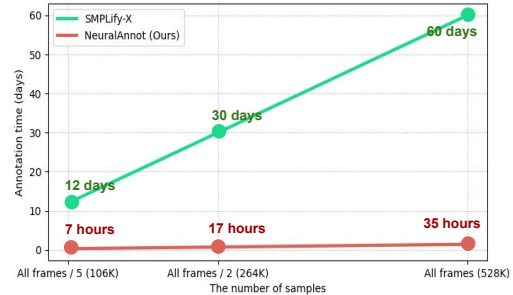


Figure 7: The annotation time comparison between SMPLify-X and NeuralAnnot on Human3.6M.

of Figure 4, while SMPLify-X cannot as it only utilizes GT 3D pose without the image input.

Both SMPLify-X and NeuralAnnot annotate 3D pseudo-GT fits using the GT 3D pose of the dataset. We ran both on only one view and uniformly sampled Human3.6M and MPI-INF-3DHP by 5 and 3 frames, respectively, following previous training set protocol [15, 18, 19, 28]. Therefore, the total numbers of samples of Human3.6M, MPI-INF-3DHP, and InterHand2.6M are 106K, 44K, and 37K, respectively. As described in Section 6.2, the annotation times of SMPLify-X are measured from a quarter of the above number of samples. The 2D/3D coordinates of other views can be obtained by applying the camera parameters provided in the dataset. We modified SMPLify-X to optimize it to GT 3D poses as the original one does not consider the 3D pose during the optimization, where its modifications are described in the supplementary material.

3D pseudo-GT fits of in-the-wild datasets. Table 4 shows that pseudo-GTs from our NeuralAnnot achieve the lowest indirect 3D annotation error and the shortest annotation time. SMPLify-X achieves the smallest 2D annotation errors, while its indirect 3D annotation errors are high. This

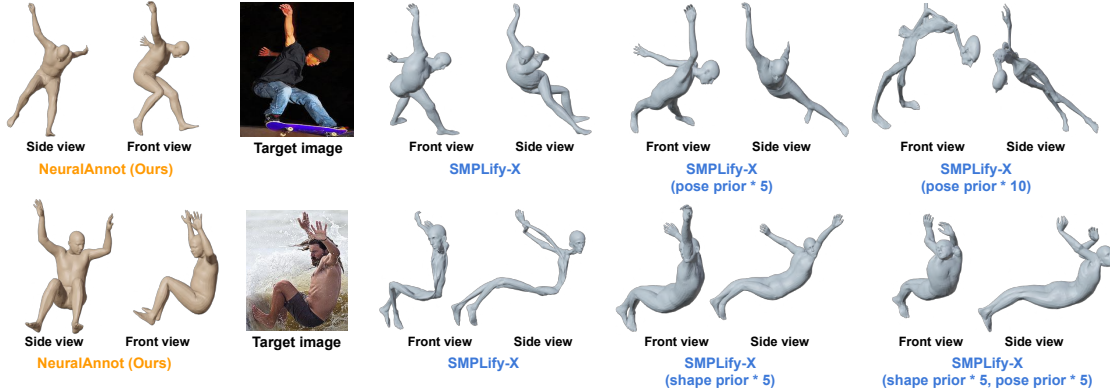


Figure 8: Qualitative comparison of expressive 3D pseudo-GTs between NeuralAnnot and SMPLify-X with various prior weights.

Annotators	2D err.	Time	Indirect 3D err.	Use in-the-wild 3D pseudo-GTs
Human body part			PA MPJPE↓	
SMPLify [4]	6.9	-	81.7	✗
SMPLify-X [32]	4.0	6 days	78.7	✗
SPIN [18]	4.8	30 days	75.4	✓
EFT [14]	5.7	30 days	69.0	✓
NeuralAnnot (Ours)	6.5	2 days	64.9	✗
Human hand part			AUC↑	
SMPLify-X [32]	6.3	4 days	0.731	✗
NeuralAnnot (Ours)	12.5	9 hours	0.780	✗

Table 4: The 2D annotation error (pixel), annotation time, and indirect 3D annotation errors comparison between MSCOCO pseudo-GTs from various annotators.

shows pseudo-GTs of SMPLify-X suffer from depth ambiguity as it relies on only 2D supervisions for the annotation. Figure 6 shows that SMPLify-X fails when the target image’s pose is far from the initial T-pose, or there is truncation. We resolve this issue by training NeuralAnnot on entire datasets with 3D supervisions from the auxiliary datasets. Figure 8 shows that simply changing hyperparameters of SMPLify-X cannot improve its results on challenging poses. SPIN [18] and EFT [14] require initial 3D pseudo-GTs of in-the-wild datasets [2, 11, 12, 23] for the training, while ours do not require. They obtained the initial 3D pseudo-GTs using SMPLify-X [32]; however, our NeuralAnnot can be used to provide better ones much faster. We think the reason for our better indirect 3D errors than SPIN and EFT is that their per-sample optimizations (*i.e.*, fitting-in-the-loop of SPIN and exemplar fine-tuning of EFT) rely only on 2D supervisions and priors without 3D supervisions. We could not compare ours with Song *et al.* [35] directly as their fits are not available; however, Table 2 and Figure 4 show the validity of taking an image as input compared with taking only pose as an input like them. Figure 9 shows failure cases of NeuralAnnot on in-the-wild images, which mostly arise from the depth ambiguity. The close body parts (first row) and challenging viewpoints (second row) are remaining hurdles to overcome, and we think

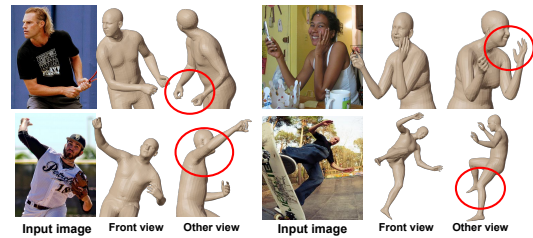


Figure 9: Failure cases of NeuralAnnot.

capturing auxiliary datasets that contain those situations can be one of the solutions.

We used SMPLify [4] fits, released by Kolotouros *et al.* [18]. The SMPLify-X fits are obtained from officially released codes, which optimizes the latent code of VPoser and PCA coefficients for the body and hand part, respectively, like ours. We used officially released SPIN [18] and EFT [14] fits. The EFT fine-tunes pre-trained SPIN [18] on each training sample. As SPIN uses initial 3D pseudo-GTs, obtained by SMPLify-X, of Human3.6M, MPI-INF-3DHP, MSCOCO, MPII [3], and LSP [11, 12] for the training, we calculated the annotation time of the SPIN and EFT by a summation of 1) SMPLify-X optimization time on the datasets for the initial 3D pseudo-GTs, 2) training time of SPIN, and 3) sample-specific fine-tuning, where the last step is included only for EFT. Each step takes 12+5+6+4+1 days, 2 days, and several hours, respectively. The annotation time of NeuralAnnot is a total time of Algorithm 1, which includes the annotation time of the auxiliary datasets and the target dataset.

7. Conclusion

We present NeuralAnnot, a neural annotator that learns to construct expressive 3D human pose and mesh training sets. Our NeuralAnnot is trained on entire datasets by considering multiple samples together, thus highly robust to the local minima and takes much shorter annotation time. Moreover, 3D supervisions from the auxiliary datasets decrease the depth ambiguity. The pseudo-GTs from Neu-

ralAnnot are demonstrated to be highly beneficial as the training sets for expressive 3D human pose and mesh estimation. We will release the newly obtained pseudo-GTs of not only datasets we used but also other various existing 2D/3D human pose and mesh datasets, not included in the paper.

Supplementary Material of “NeuralAnnot: Neural Annotator for in-the-wild Expressive 3D Human Pose and Mesh Training Sets”

In this supplementary material, we present more experimental results that could not be included in the main manuscript due to the lack of space.

8. Improving bad 3D pseudo-GTs of NeuralAnnot

Although NeuralAnnot provides beneficial 3D pseudo-GTs effectively and efficiently, some of 3D pseudo-GTs are bad due to the depth ambiguity. This is because samples of in-the-wild datasets are supervised only by 2D loss functions without 3D supervisions. To resolve this issue, we supervise samples of the in-the-wild dataset using 3D pseudo-GTs, following SPIN [18] and EFT [14]. Unlike SPIN [18] and EFT [14] used outputs of SMPLify-X [32] as the 3D pseudo-GTs of in-the-wild datasets, we use outputs of our NeuralAnnot as the 3D pseudo-GTs. To this end, we first train and test NeuralAnnot to obtain 3D pseudo-GTs of all auxiliary and in-the-wild datasets. Then, we randomly initialize NeuralAnnot and re-train it by supervising it using the obtained 3D pseudo-GTs of the auxiliary and in-the-wild datasets. The first and second rounds used the same datasets; however, the first round of NeuralAnnot training does not use 3D pseudo-GTs of the in-the-wild dataset, while the second round of the training uses it. Table 5 and Figure 10 shows that using 3D pseudo-GTs of in-the-wild dataset greatly improves the quality of 3D pseudo-GTs. As most of the 3D pseudo-GTs from the first round of NeuralAnnot training provide accurate 3D pose and mesh, supervising samples of the in-the-wild dataset by the 3D pseudo-GTs of the first round can teach NeuralAnnot to reason 3D information from the in-the-wild images.

9. In-depth comparison with SMPLify-X

9.1. Data-driven learning vs. per-sample optimization

We think NeuralAnnot has a higher potential to provide better pseudo-GTs than SMPLify-X when 1) the target task is highly ill-posed and 2) there are many prepared data. Recovering 3D human *body and hand* model fits from 1) GT 2D poses, 2) GT 3D poses, 3) pairs of images and GT 2D poses, or 4) pairs of images and GT 3D poses satisfy the above conditions. The human body and hand have highly complicated articulations; therefore, recovering their fits from the above data involves ill-posedness, and the ill-posedness becomes severe when the 3D data are not available. As the inputs of ill-posed problems do not contain perfect information to recover outputs, the system should be robust to diverse input patterns. NeuralAnnot alleviates the

3D pseudo-GTs of in-the-wild datasets	Indirect 3D err.
No	64.9
From NeuralAnnot	62.4

Table 5: Indirect 3D annotation error comparison between models without and with 3D pseudo-GTs of in-the-wild datasets on 3DPW.

Annotators	Knees	Ankles	Elbows	Wrists	All
SMPLify-X [32]	16.6	9.6	10.0	8.9	13.1
NeuralAnnot (Ours)	15.0	9.5	5.8	7.2	9.8

Table 6: The direct 3D annotation error of major joints comparison between SMPLify-X and NeuralAnnot on Human3.6M. The errors of left and right joints are averaged.

Annotators	Indirect 3D err. (mm)	Time
SMPLify-X [32]	2.06	16 hours
NeuralAnnot (Ours)	2.09	6 hours

Table 7: Indirect 3D annotation error (mm) of the face part comparison between SMPLify-X [32] and NeuralAnnot on Stirling.

above issue by updating its learnable weights from diverse patterns of many data, which makes NeuralAnnot produces robust outputs from diverse input patterns. On the other hand, SMPLify-X does not learn diverse patterns of many data; instead, it optimizes a 3D human model to each data independently, which makes it fail to produce robust outputs from diverse inputs. We utilize large-scale 2D/3D pose datasets [2, 9, 11, 12, 23, 26, 30] to train NeuralAnnot, which make NeuralAnnot produce robust 3D pseudo-GTs from diverse inputs.

9.2. 3D pseudo-GTs from datasets with GT 3D pose.

Table 6 shows NeuralAnnot achieves lower direct 3D annotation error for all major joints.

9.3. 3D pseudo-GTs from in-the-wild dataset.

Figure 11 shows NeuralAnnot produces far better 3D body and hand pseudo-GTs than SMPLify-X.

9.4. Qualitative comparison of 3D face pseudo-GTs

Table 7 shows SMPLify-X achieves slightly better indirect 3D annotation error for the face part. Figure 12 shows NeuralAnnot and SMPLify-X produce similar 3D face pseudo-GTs. The bottom row of the figure shows failure cases of both approaches. The first column is a failure from challenging face direction, and the second column is a failure of the delicate facial expression capture. Unlike the body and hand parts, the face part does not involve complicated articulation, which makes SMPLify-X work well and produce similar or slightly better results to those of NeuralAnnot.

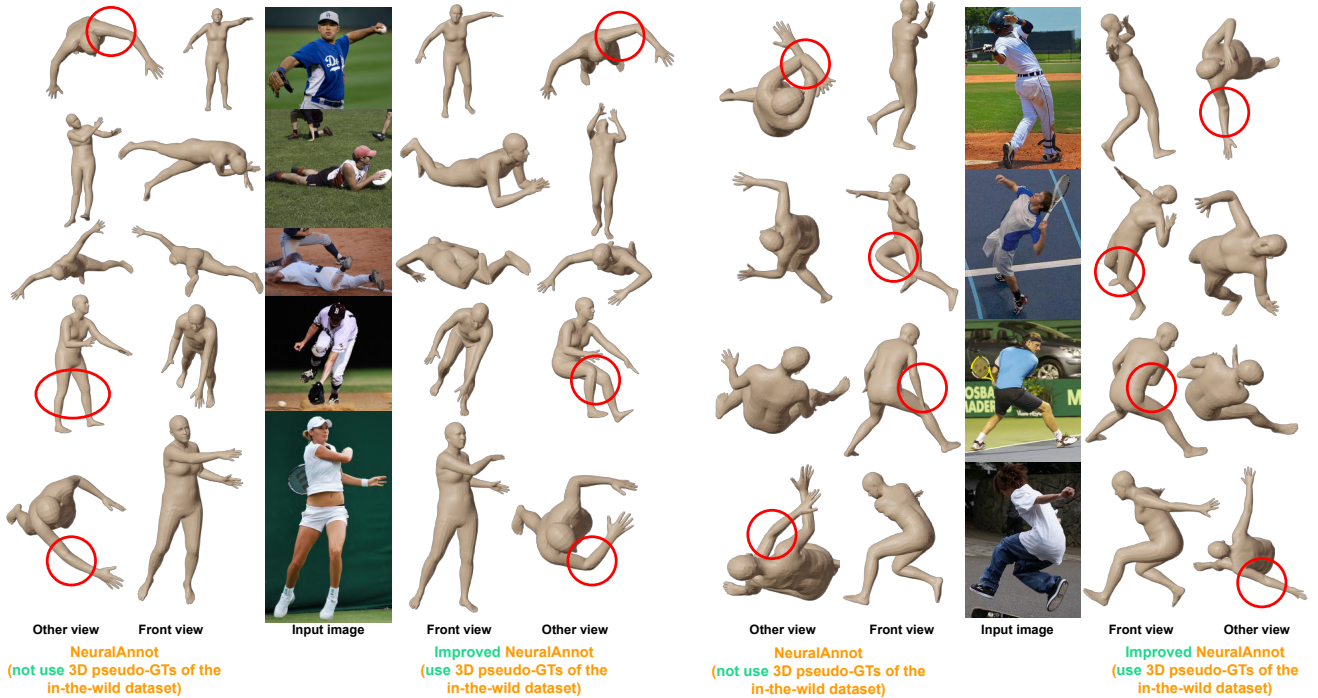


Figure 10: Qualitative comparison between NeuralAnnot trained without and with 3D pseudo-GTs of the in-the-wild dataset on MSCOCO. The 3D pseudo-GTs of the in-the-wild dataset are obtained by our NeuralAnnot.

10. Qualitative comparison with EFT

Figure 13 shows NeuralAnnot is more robust to truncation and invisible joints than EFT [14]. EFT fine-tunes a pre-trained network [18] on the GT 2D pose of each image, and missing annotations in GT 2D due to the truncation and occlusions make their result unstable. In addition, as they use outputs of SMPLify-X [32] as 3D pseudo-GTs to train their network, wrong fits of SMPLify-X, shown in Figure 11, can affect their performance.

11. Qualitative results on challenging images

Figure 14 shows our NeuralAnnot is highly robust to occlusions and truncation in crowd scenes of CrowdPose [21].

12. Comparison with previous annotators using a different estimator

Table 8 shows 3D pseudo-GTs from NeuralAnnot still achieves the best indirect 3D errors, where the indirect 3D errors are calculated from a different estimator compared with I2L-MeshNet [28] of the main manuscript. For the new estimator, we used a network similar to HMR [15] and SPIN [18], which regresses SMPL parameters from the global average pooled ResNet output feature vector. The new estimator is a model-based approach, which regresses 3D human model parameters, while I2L-MeshNet [28] is a

Annotators	2D err.	Time	Indirect 3D err.	Use in-the-wild 3D pseudo-GTs
			PA MPJPE↓	
<i>Human body part</i>				
SMPLify [4]	6.9	-	85.1	✗
SMPLify-X [32]	4.0	6 days	79.4	✗
SPIN [18]	4.8	30 days	77.1	✓
EFT [14]	5.7	30 days	71.6	✓
NeuralAnnot (Ours)	6.5	2 days	68.3	✗
			AUC↑	
<i>Human hand part</i>				
SMPLify-X [32]	6.3	4 days	0.755	✗
NeuralAnnot (Ours)	12.5	9 hours	0.786	✗

Table 8: The 2D annotation error (pixel), annotation time, and indirect 3D annotation errors comparison between MSCOCO pseudo-GTs from various annotators.

model-free approach, which regresses 3D mesh vertex coordinates. As the two estimators are based on a very different approach, we can conclude that 3D pseudo-GTs of our NeuralAnnot are highly beneficial than those of previous annotators regardless of the estimator type.

13. Optimizing SMPLify-X on 3D pose

As original SMPLify-X does not consider 3D pose during the optimization, we modified it to consider 3D pose for 3D pseudo-GTs of Human3.6M [9], MPI-INF-3DHP [26], and InterHand2.6M [30], which provide GT 3D poses. The modified SMPLify-X optimizes 3D human model (*i.e.*, one of SMPL [25], MANO [33], FLAME [22], and SMPL-

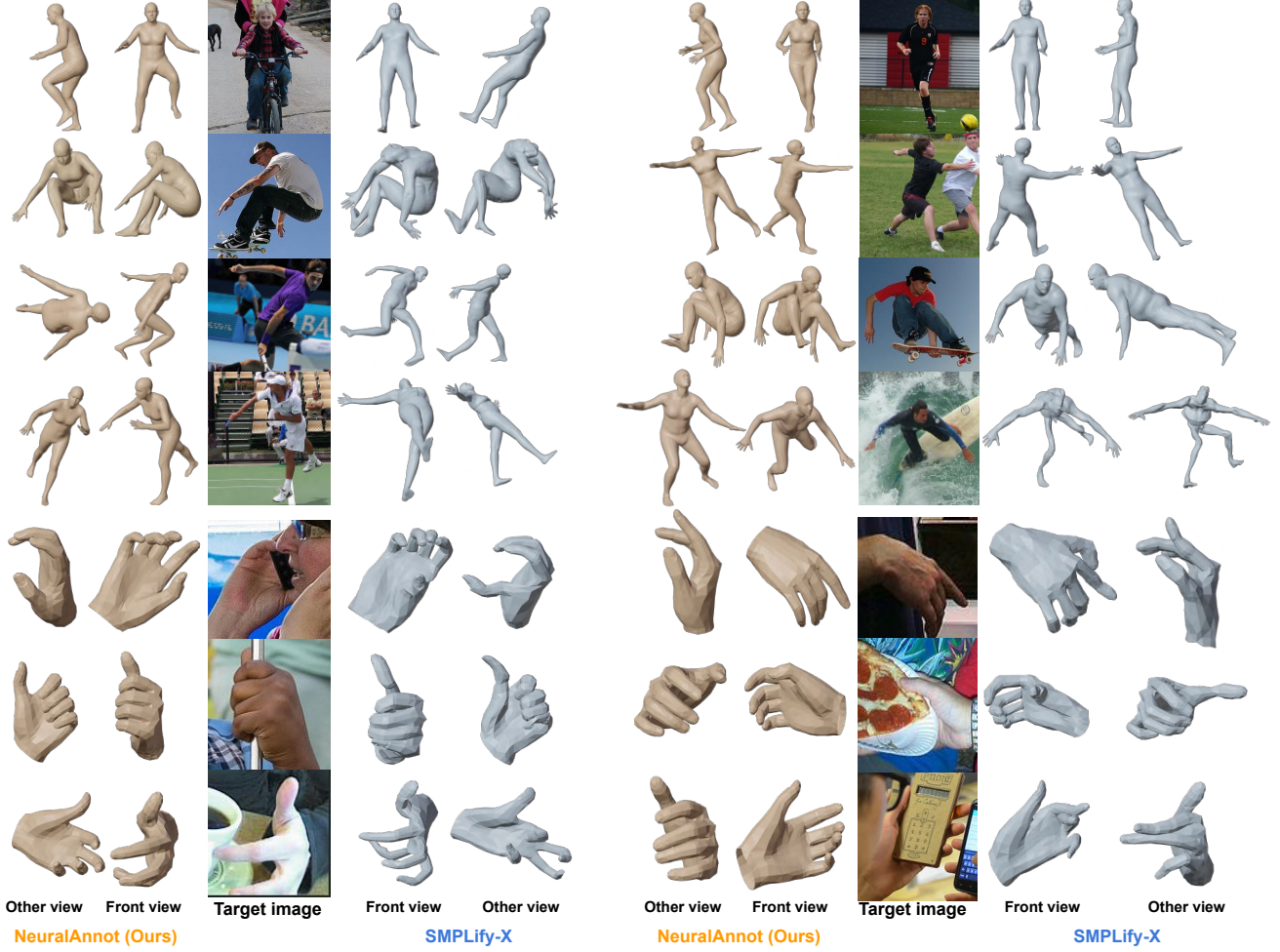


Figure 11: Qualitative comparison between 3D body and hand pseudo-GTs of NeuralAnnot and SMPLify-X on MSCOCO.

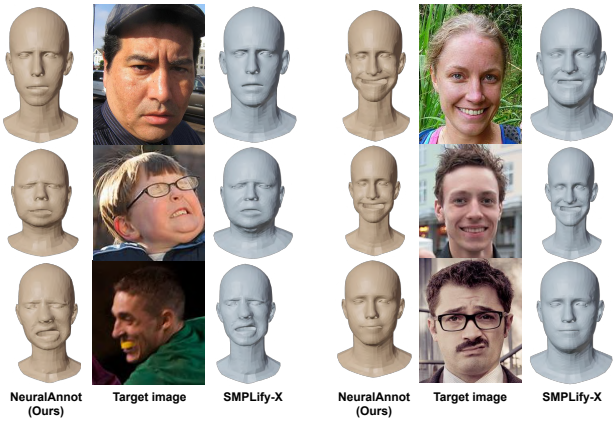


Figure 12: Qualitative comparison between 3D face pseudo-GTs of NeuralAnnot and SMPLify-X on MSCOCO.

X [32]) to 3D camera-centered coordinates of human joints. To this end, we made two modifications.

Camera initialization. The original SMPLify-X uses fixed intrinsic camera parameters (*i.e.*, focal lengths and principal points) and initializes a 3D translation vector based on 2D target joint positions. The obtained 3D translation vector is used to project 3D joint coordinates from a fit to the 2D space using a perspective projection. On the other hand, the target is 3D in this case, not 2D; therefore, we discard the intrinsics and the 3D translation vector. Instead, we initialize extrinsic camera parameters R and t using hip and shoulder 3D joint coordinates by performing SVD. R and t represent a 3D rotation matrix and 3D translation vector, respectively, from a human model coordinate system to a dataset coordinate system. We chose the hip and shoulder joints as they can roughly decide the 3D global rotations of human body, while end-point joints (*e.g.*, wrists and ankles) cannot.

3D data term. We changed the 2D pose-based data term of

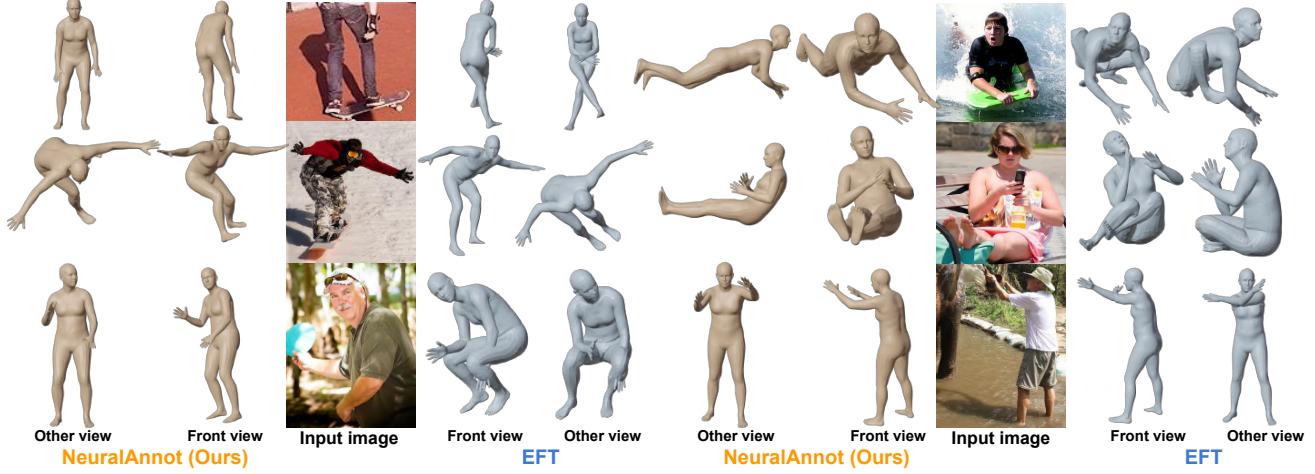


Figure 13: Qualitative comparison between NeuralAnnot and EFT [14] on MSCOCO.

SMPLify-X to the 3D pose-based term, which calculates a distance between the GT 3D pose of Human3.6M and 3D joint coordinates from a fit. We use a Geman-McClure error function [7] for the distance used in the 2D pose-based data term of the original SMPLify-X. We tried several other distances, such as $L1$ and $L2$, and found that Geman-McClure error function [7] and $L1$ work the best. The distance is calculated in a meter scale, and we set the weight of the data term to 10^6 , which works the best. The 3D joint coordinates from a fit are obtained by multiplying a joint regression matrix of Human3.6M to a mesh. The matrix defines a linear relationship between a SMPL mesh and Human3.6M 17 joints, and we used a released matrix of Bogo *et al.* [4].

14. Comparison with state-of-the-art estimators

Table 9 shows that I2L-MeshNet trained on pseudo-GTs obtained by our NeuralAnnot significantly outperforms all previous methods, including original I2L-MeshNet trained on pseudo-GTs obtained by SMPLify-X. Table 10 shows that a regressor trained on pseudo-GTs obtained by our NeuralAnnot outperforms all previous methods on all human parts. The regressor has a simple network architecture, similar to that of ExPose [6], and its detailed descriptions are provided below. Without bells and whistles, we achieved state-of-the-art performance on body-only and expressive datasets using pseudo-GTs obtained by our NeuralAnnot. This clearly shows that pseudo-GTs from our NeuralAnnot are highly beneficial for the training.

The regressor has exactly the same network architecture as NeuralAnnot. There are three sub-networks for the body, hand, and face parts in the regressor. Each subnetwork consists of ResNet [8] and several fully connected layers for the human model parameter prediction. We train each sub-

Methods	Pseudo-GTs from	MPJPE	PA MPJPE
HMR [15]	Mosh [24]	130.0	81.3
GraphCMR [19]	Mosh [24]	-	70.2
SPIN [18]	Mosh [24]+SMPLify [4]	96.9	59.2
ExPose [6]	SMPLify-X [32]	93.4	60.7
Pose2Mesh [5]	SMPLify-X [32]	88.9	58.3
I2L-MeshNet [28]	SMPLify-X [32]	93.2	57.7
	NeuralAnnot (Ours)	86.6	54.3

Table 9: MPJPE and PA MPJPE comparison on 3DPW.

Methods	PA MPVPE			PA MPJPE	
	All	Hands	Face	Body	Hands
SMPLify-X [32]	65.3	12.3	6.3	87.6	12.9
MTC [37]	67.2	-	-	107.8	16.7
ExPose [6]	54.5	12.8	5.8	62.8	13.1
Regressor (Ours)	53.5	12.0	5.7	61.4	11.7

Table 10: PA MPVPE and PA MPJPE comparison on EHF. The numbers in hands are averaged values of left and right hands.

Settings	2D err.	Indirect 3D err.
Without VPoser	5.0	113.5
With VPoser (Ours)	8.1	65.9

Table 11: The 2D annotation error (pixel) and indirect 3D annotation error (PA MPJPE) comparison between MSCOCO pseudo-GTs from various settings of NeuralAnnot.

network separately, and the loss function is a $L1$ distance between predicted and GT human model parameters and 2D/3D coordinates, similar to Kolotouros *et al.* [18]. For the final expressive 3D human pose and mesh, we integrate outputs of each sub-network using the integration module of Section 16.

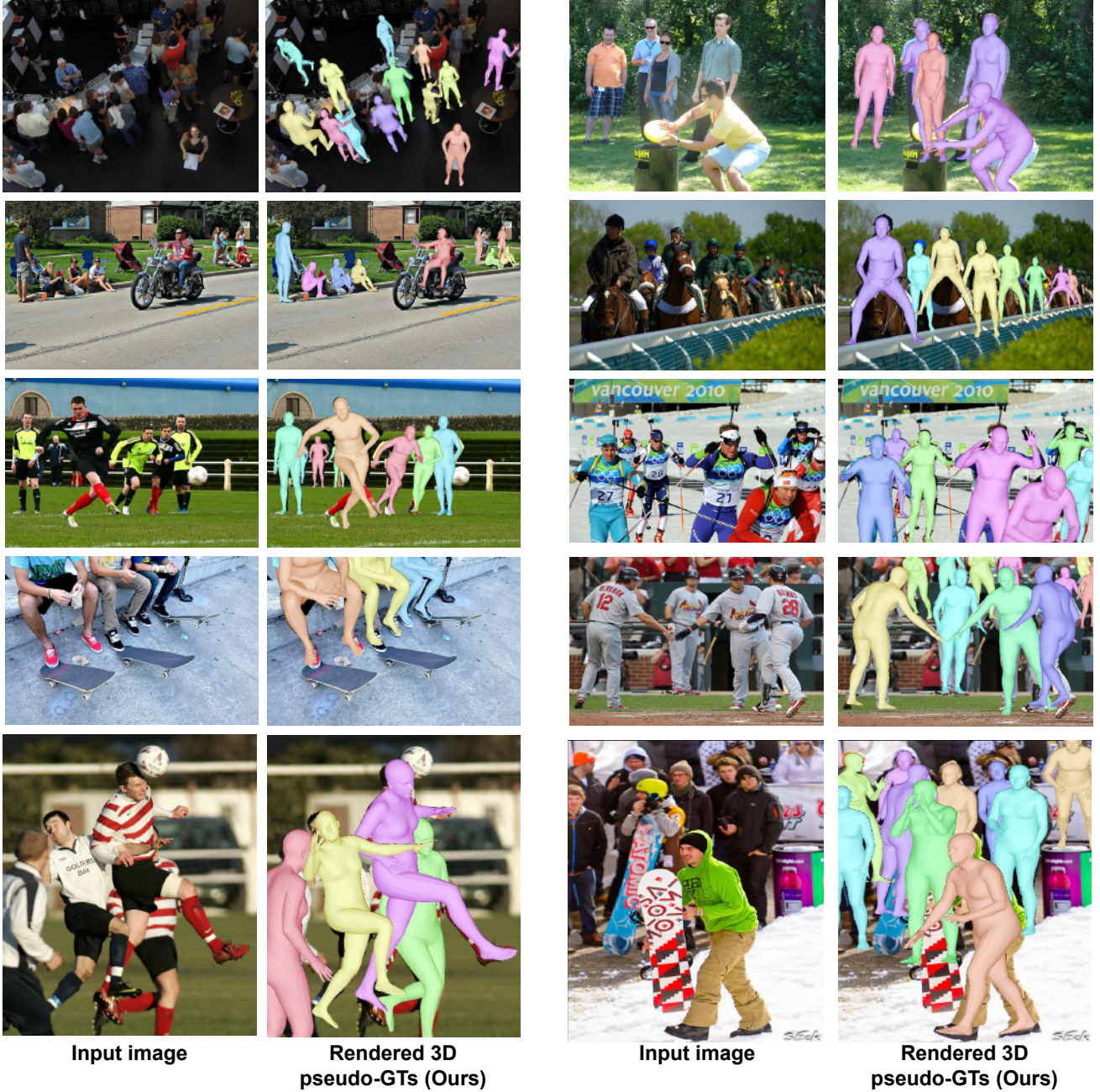


Figure 14: Visualized 3D body pseudo-GTs of NeuralAnnot on CrowdPose. NeuralAnnot is robust to truncation and occlusions.

15. Benefit of the low-dimensional embedded pose prediction.

Table 11 shows predicting the low-dimensional embedded pose (*i.e.*, the latent code of VPoser for the body part) when minimizing L_{tg} largely decreases the indirect 3D annotation error. Interestingly, the 2D annotation error becomes smaller when the low-dimensional embedded pose

is not used, while its indirect 3D annotation error increases. This indicates that the low-dimensional pose makes the system suffer less from depth ambiguity by effectively preventing implausible poses with very simple regularizers (*i.e.*, L_2 regularizer for ours). For all settings, MPI-INF-3DHP is used as the auxiliary dataset. When VPoser is not used, the pose is initially predicted in a 6D rotational representation [40] and converted to the 3D axis-angle following [18].

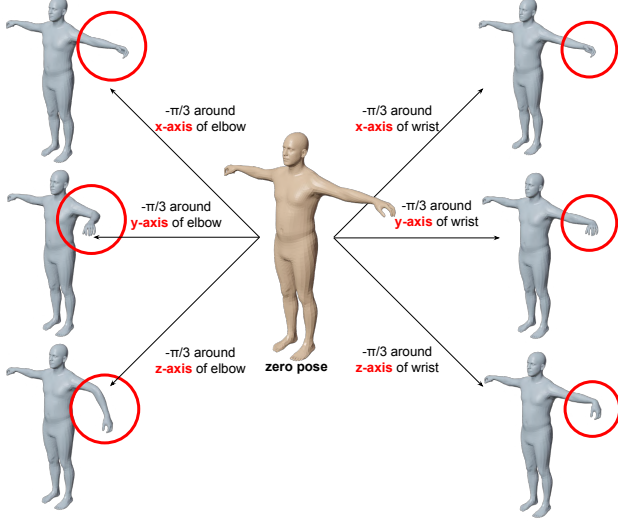


Figure 15: Visualized rotations of the elbow and wrist in each axis.

The same tendency was observed for the hand part by predicting the PCA coefficients of the hand pose space.

16. All parts integration module

As described in Section 4 of the main manuscript, we selectively use global rotations of right and left hands, θ_{rh}^g and θ_{lh}^g , respectively, when integrating outputs of networks of each part. Algorithm 2 and Figure 15 show the integration procedure and how rotations of elbow and wrist change the body, respectively. First, we perform forward kinematics to compute global rotations of all body joints, including wrists and elbows (line 1). Then, we replace the global rotations of wrists and elbows using the global rotation of hands (lines 4 and 5). The replacement assumes x -axis rotations (roll of Euler angle) of the wrist and elbow are almost the same, which follows the anatomical structure of the human body, as shown in Figure 15. To avoid a sudden change of the elbow rotation, which can cause artifacts, we use an average rotation of the elbow and wrist (line 5). From the replaced global rotations of wrists and elbows, we compute new local rotations of wrists and elbows (line 6). Finally, we check the new local rotation follows the anatomical structure of the human body (line 7), where y - and z -axis rotations are shown in Figure 15. If true, we update the local rotations of body joints, which become the final output of the integration (lines 8 and 9). We convert the 3D rotation of joints to Euler angles in line 3 - line 11. Figure 16 shows that our integration algorithm changes 3D elbow rotation (lines 4 and 5), and our anatomical prior (line 7) prevents implausible 3D wrist rotation.

Algorithm 2 Integration of body and hands

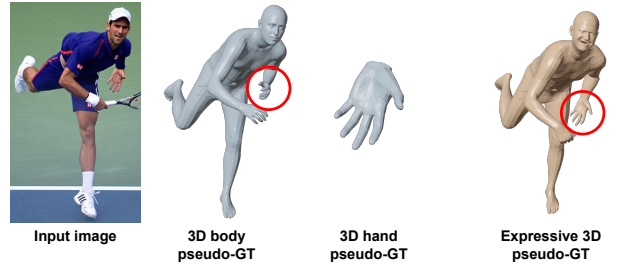
Input: θ_b^g : Global rotation of body

Input: $\theta_b^l = \{\theta_j^l\}_{j=1}^{21}$: Local rotations of body joints

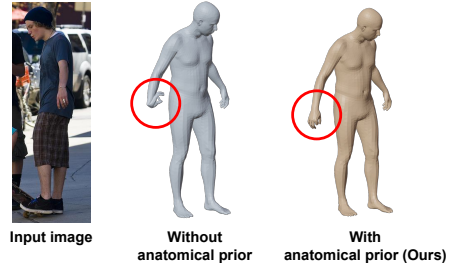
Input: $\theta_{rh}^g, \theta_{lh}^g$: Global rotations of right and left hands

Output: θ_b : Updated local rotations of body joints

- 1: Compute global rotations of body joints $\{\theta_j^g\}_{j=1}^{21}$ from θ_b^g and θ_b by forward kinematics
- 2: Let re, le, rw, lw denote joint index of right elbow, left elbow, right wrist, and left wrist, respectively.
- 3: **for** $(e, w, h) \leftarrow ((re, rw, rh), (le, lw, lh))$ **do**
- 4: $\theta_w^g \leftarrow \theta_h^g$
- 5: $x\text{-axis of } \theta_e^g \leftarrow x\text{-axis of } (\theta_e^g + \theta_h^g)/2$
- 6: Compute new local rotations of elbow and wrist, $\hat{\theta}_e^l$ and $\hat{\theta}_w^l$, respectively, from $\{\theta_j^g\}_{j=1}^{21}$ by reversing forward kinematics
- 7: **if** $|y\text{-axis of } \hat{\theta}_w^l| < \pi/4$ and $|z\text{-axis of } \hat{\theta}_w^l| < \pi/2$ **then**
- 8: Update $\theta_w^l \leftarrow \hat{\theta}_w^l$
- 9: Update $\theta_e^l \leftarrow \hat{\theta}_e^l$
- 10: **end if**
- 11: **end for**



(a) Effectiveness of the elbow rotation replacement during the part integration



(b) Effectiveness of the anatomical prior during the part integration

Figure 16: (a) Our part integration algorithm changes 3D elbow rotation using 3D hand global rotation. (b) Our anatomical prior during the integration prevents implausible 3D wrist rotations.

References

- [1] Mykhaylo Andriluka, Umar Iqbal, Eldar Insafutdinov, Leonid Pishchulin, Anton Milan, Juergen Gall, and Bernt Schiele. PoseTrack: A benchmark for human pose estima-

- tion and tracking. In *CVPR*, 2018. 2
- [2] Mykhaylo Andriluka, Leonid Pishchulin, Peter Gehler, and Bernt Schiele. 2D human pose estimation: New benchmark and state of the art analysis. In *CVPR*, 2014. 1, 2, 3, 8, 10
- [3] Mykhaylo Andriluka, Leonid Pishchulin, Peter Gehler, and Bernt Schiele. 2D human pose estimation: New benchmark and state of the art analysis. In *CVPR*, 2014. 2, 8
- [4] Federica Bogo, Angjoo Kanazawa, Christoph Lassner, Peter Gehler, Javier Romero, and Michael J Black. Keep it SMPL: Automatic estimation of 3D human pose and shape from a single image. In *ECCV*, 2016. 2, 3, 5, 8, 11, 13
- [5] Hongsuk Choi, Gyeongsik Moon, and Kyoung Mu Lee. Pose2Mesh: Graph convolutional network for 3D human pose and mesh recovery from a 2D human pose. In *ECCV*, 2020. 6, 13
- [6] Vasileios Choutas, Georgios Pavlakos, Timo Bolkart, Dimitrios Tzionas, and Michael J Black. Monocular expressive body regression through body-driven attention. In *ECCV*, 2020. 3, 13
- [7] Stuart Geman. Statistical methods for tomographic image reconstruction. *Bull. Int. Stat. Inst.*, 1987. 13
- [8] Kaifeng He, Xiangyu Zhang, Shaoqing Ren, and Jian Sun. Deep residual learning for image recognition. In *CVPR*, 2016. 3, 5, 13
- [9] Catalin Ionescu, Dragos Papava, Vlad Olaru, and Cristian Sminchisescu. Human3.6M: Large scale datasets and predictive methods for 3D human sensing in natural environments. *TPAMI*, 2014. 1, 2, 3, 4, 5, 6, 7, 10, 11
- [10] Sheng Jin, Lumin Xu, Jin Xu, Can Wang, Wentao Liu, Chen Qian, Wanli Ouyang, and Ping Luo. Whole-body human pose estimation in the wild. In *ECCV*, 2020. 2, 5
- [11] Sam Johnson and Mark Everingham. Clustered pose and nonlinear appearance models for human pose estimation. In *BMVC*, 2010. 1, 2, 3, 8, 10
- [12] Sam Johnson and Mark Everingham. Learning effective human pose estimation from inaccurate annotation. In *CVPR*, 2011. 1, 2, 3, 8, 10
- [13] Hanbyul Joo, Hao Liu, Lei Tan, Lin Gui, Bart Nabbe, Iain Matthews, Takeo Kanade, Shohei Nobuhara, and Yaser Sheikh. Panoptic Studio: A massively multiview system for social motion capture. In *ICCV*, 2015. 1, 2
- [14] Hanbyul Joo, Natalia Neverova, and Andrea Vedaldi. Exemplar fine-tuning for 3D human pose fitting towards in-the-wild 3D human pose estimation. *arXiv preprint arXiv:2004.03686*, 2020. 3, 8, 10, 11, 13
- [15] Angjoo Kanazawa, Michael J Black, David W Jacobs, and Jitendra Malik. End-to-end recovery of human shape and pose. In *CVPR*, 2018. 1, 7, 11, 13
- [16] Tero Karras, Samuli Laine, and Timo Aila. A style-based generator architecture for generative adversarial networks. In *CVPR*, 2019. 2
- [17] Diederik P Kingma and Jimmy Ba. Adam: A method for stochastic optimization. In *ICLR*, 2014. 5
- [18] Nikos Kolotouros, Georgios Pavlakos, Michael J Black, and Kostas Daniilidis. Learning to reconstruct 3D human pose and shape via model-fitting in the loop. In *ICCV*, 2019. 3, 6, 7, 8, 10, 11, 13, 14
- [19] Nikos Kolotouros, Georgios Pavlakos, and Kostas Daniilidis. Convolutional mesh regression for single-image human shape reconstruction. In *CVPR*, 2019. 1, 7, 13
- [20] Dominik Kulon, Riza Alp Guler, Iasonas Kokkinos, Michael M Bronstein, and Stefanos Zafeiriou. Weakly-supervised mesh-convolutional hand reconstruction in the wild. In *CVPR*, 2020. 2
- [21] Jiefeng Li, Can Wang, Hao Zhu, Yihuan Mao, Hao-Shu Fang, and Cewu Lu. CrowdPose: Efficient crowded scenes pose estimation and a new benchmark. In *CVPR*, 2019. 11
- [22] Tianye Li, Timo Bolkart, Michael J Black, Hao Li, and Javier Romero. Learning a model of facial shape and expression from 4D scans. *ACM TOG*, 2017. 1, 4, 11
- [23] Tsung-Yi Lin, Michael Maire, Serge Belongie, James Hays, Pietro Perona, Deva Ramanan, Piotr Dollár, and C Lawrence Zitnick. Microsoft COCO: Common objects in context. In *ECCV*, 2014. 1, 2, 3, 4, 5, 8, 10
- [24] Matthew Loper, Naureen Mahmood, and Michael J Black. MoSh: Motion and shape capture from sparse markers. *ACM TOG*, 2014. 13
- [25] Matthew Loper, Naureen Mahmood, Javier Romero, Gerard Pons-Moll, and Michael J Black. SMPL: A skinned multi-person linear model. *ACM TOG*, 2015. 1, 2, 4, 11
- [26] Dushyant Mehta, Helge Rhodin, Dan Casas, Pascal Fua, Oleksandr Sotnychenko, Weipeng Xu, and Christian Theobalt. Monocular 3D human pose estimation in the wild using improved cnn supervision. In *3DV*, 2017. 1, 2, 3, 4, 5, 6, 7, 10, 11
- [27] Dushyant Mehta, Oleksandr Sotnychenko, Franziska Mueller, Weipeng Xu, Srinath Sridhar, Gerard Pons-Moll, and Christian Theobalt. Single-shot multi-person 3D pose estimation from monocular RGB. In *3DV*, 2018. 2
- [28] Gyeongsik Moon and Kyoung Mu Lee. I2L-MeshNet: Image-to-Lixel prediction network for accurate 3D human pose and mesh estimation from a single RGB image. In *ECCV*, 2020. 1, 6, 7, 11, 13
- [29] Gyeongsik Moon and Kyoung Mu Lee. Pose2Pose: 3D positional pose-guided 3D rotational pose prediction for expressive 3d human pose and mesh estimation. *arXiv preprint arXiv:2011.11534*, 2020. 3
- [30] Gyeongsik Moon, Shoou-I Yu, He Wen, Takaaki Shiratori, and Kyoung Mu Lee. InterHand2.6M: A dataset and baseline for 3D interacting hand pose estimation from a single RGB image. In *ECCV*, 2020. 1, 2, 4, 5, 6, 7, 10, 11
- [31] Adam Paszke, Sam Gross, Soumith Chintala, Gregory Chanan, Edward Yang, Zachary DeVito, Zeming Lin, Alban Desmaison, Luca Antiga, and Adam Lerer. Automatic differentiation in pytorch. 2017. 5
- [32] Georgios Pavlakos, Vasileios Choutas, Nima Ghorbani, Timo Bolkart, Ahmed AA Osman, Dimitrios Tzionas, and Michael J Black. Expressive body capture: 3D hands, face, and body from a single image. In *CVPR*, 2019. 1, 2, 3, 4, 5, 6, 7, 8, 10, 11, 12, 13
- [33] Javier Romero, Dimitrios Tzionas, and Michael J Black. Embodied Hands: Modeling and capturing hands and bodies together. *ACM TOG*, 2017. 1, 2, 4, 11

- [34] Olga Russakovsky, Jia Deng, Hao Su, Jonathan Krause, Sanjeev Satheesh, Sean Ma, Zhiheng Huang, Andrej Karpathy, Aditya Khosla, Michael Bernstein, et al. ImageNet large scale visual recognition challenge. *IJCV*, 2015. 5
- [35] Jie Song, Xu Chen, and Otmar Hilliges. Human body model fitting by learned gradient descent. In *ECCV*, 2020. 3, 6, 8
- [36] Timo von Marcard, Roberto Henschel, Michael J Black, Bodo Rosenhahn, and Gerard Pons-Moll. Recovering accurate 3D human pose in the wild using IMUs and a moving camera. In *ECCV*, 2018. 2, 5, 6
- [37] Donglai Xiang, Hanbyul Joo, and Yaser Sheikh. Monocular Total Capture: Posing face, body, and hands in the wild. In *CVPR*, 2019. 13
- [38] Zhixuan Yu, Jae Shin Yoon, In Kyu Lee, Prashanth Venkatesh, Jaesik Park, Jihun Yu, and Hyun Soo Park. HUMBI: A large multiview dataset of human body expressions. In *CVPR*, 2020. 1
- [39] Weiyu Zhang, Menglong Zhu, and Konstantinos G Derpanis. From actemes to action: A strongly-supervised representation for detailed action understanding. In *ICCV*, 2013. 2
- [40] Yi Zhou, Connelly Barnes, Jingwan Lu, Jimei Yang, and Hao Li. On the continuity of rotation representations in neural networks. In *CVPR*, 2019. 4, 14
- [41] Christian Zimmermann, Duygu Ceylan, Jimei Yang, Bryan Russell, Max Argus, and Thomas Brox. FreiHAND: A dataset for markerless capture of hand pose and shape from single RGB images. In *ICCV*, 2019. 2, 5, 6